FBMC Receiver Design and Analysis for Medium and Large Scale Antenna Systems

Hamed Hosseiny[†], Arman Farhang[*] and Behrouz Farhang-Boroujeny[†]

[†]ECE Department, University of Utah, USA,

[*]Department of Electronic and Electrical Engineering, Trinity College Dublin, Ireland.

Email: {hamed.hosseiny, farhang}@utah.edu, {arman.farhang}@tcd.ie

Abstract—In this paper, we design receivers for filter bank multicarrier-based (FBMC-based) massive MIMO considering practical aspects such as channel estimation and equalization. In particular, we propose a spectrally efficient pilot structure and a channel estimation technique in the uplink to jointly estimate all the users' channel impulse responses. We mathematically analyze our proposed channel estimator and find the statistics of the channel estimation errors. These statistics are incorporated into our proposed equalizers to deal with the imperfect channel state information (CSI) effect. We revisit the channel equalization problem for FBMC-based massive MIMO, address the shortcomings of the existing equalizers in the literature, and make them more applicable to practical scenarios. The proposed receiver in this paper consists of two stages. In the first stage, a linear combining of the received signals at the base station (BS) antennas provides a coarse channel equalization and removes any multiuser interference. In the second stage, a per subcarrier fractionally spaced equalizer (FSE) takes care of any residual distortion of the channel for the user of interest. We propose an FSE design based on the equivalent channel at the linear combiner output. This enables the applicability of our proposed technique to small and/or distributed antenna setups such as cell-free massive MIMO. Finally, the efficacy of the proposed techniques is corroborated through numerical analysis.

Index Terms—FBMC, multiuser, time domain channel estimation, equalization, massive MIMO, distributed antenna, cell-free.

I. INTRODUCTION

THE emergence of new applications and technologies such as high data rate holographic communications and low latency high mobility communications for autonomous driving, as well as massive machine-type communications, has marked a new era in communications, [1]. This calls for the development of a flexible air interface in different levels and the associated modulation scheme to deliver unprecedented levels of connectivity, reliability, and flexibility, often supplemented with strict latency requirements. Even though orthogonal frequency division multiplexing (OFDM) has been chosen for the physical layer of both 4G and 5G systems, its

shortcomings, such as its sensitivity to frequency errors and bandwidth efficiency loss due to the redundant cyclic prefix (CP) and high out-of-band emissions motivate consideration of other alternative waveforms. Its high spectral efficiency and flexibility in prototype filter design to serve a diverse set of applications in future networks make filter bank multicarrier (FBMC) a promising candidate waveform for future wireless systems [2], [3].

Design of novel physical layer technologies and flexible modulation schemes such as FBMC that are bolstered with advanced co-located/distributed multiple antenna systems contribute towards an increased capacity and reliability in the future multiuser networks. The authors in [4] and [5] studied these systems and demonstrated the self-equalization/channel-flattening effect of FBMC in massive MIMO channels. In a more recent work, [6], it was noted that the channel-flattening effect of FBMC that was first reported in [7] is limited and, thus, a more accurate equalization method was needed. In particular, it was shown that this limit is the result of the correlation between combiner taps and channel impulse responses between the user terminal and the base station (BS) antennas, [6]. It was further shown that this correlation converges to an equivalent channel which resembles the power delay profile (PDP) of the set of channels between the user of interest and the BS antennas. This finding was then used to propose a per-subcarrier per-user equalizer that recovers the Nyquist property that was broken by this PDP channel.

The authors in [8] use concepts in random matrix theory to obtain the asymptotic performance of FBMC-based massive MIMO systems with a linear combiner, similar to those in [4] and [5], and presented the mean squared error (MSE) of the recovered data symbols. These results show that the MSE saturates to a lower bound and becomes uniform across all the subcarriers. Taking note that the MSE and signal-to-interference plus noise ratio (SINR) are inversely related, one may realize that this result is inline with the results of [6]. The authors in [9], on the other hand, analyze the performance of FBMC in multiuser massive MIMO systems with co-located antennas and derive lower bound expressions for achievable sum-rates with and without perfect channel state information (CSI) in the uplink when a linear combiner is deployed. The results in this paper are also in line with those in [6] and [8].

It is well known that, accurate estimates of the underlying channels are required at the BS to deliver the promising benefits of massive MIMO systems. Furthermore, many of

the emerging applications in future wireless networks require ultra-reliable low-latency communications (URLLC), [10]. This necessitates the need for highly accurate channel estimation techniques with minimal training overheads, especially in multiuser scenarios. In addition, the current literature on FBMC-based massive MIMO is mainly focused on asymptotic analysis, without much focus on the practical aspects, [6], [8], [9]. In particular, to the best of our knowledge, there is no published work to date that extensively addresses the practical problems of channel estimation that were noted above, e.g., equalization in the presence of imperfect CSI, as well as the scenarios where the number of BS antennas are limited.

The focus of this paper is on the design of a practical receiver for FBMC-based massive MIMO systems in the presence of imperfect CSI. We start with the channel estimation problem in the uplink of a FBMC-based network. We note that, in FBMC, subcarriers are orthogonal in the real field. This makes channel estimation a more complex task when compared to its OFDM counterpart. Existing channel estimation methods for FBMC are mainly based on the interference approximation method (IAM), e.g., see [11]. IAM is a frequency domain channel estimation technique and requires the maximum channel delay spread to be much shorter than the symbol interval. Thus, when this condition does not hold, IAM leads to inaccurate channel estimates. A review of the IAM-based channel estimation for FBMC is provided in [12]. Similar to single user systems, most of the channel estimation techniques for MIMO-FBMC systems are also based on the IAM model. To avoid the issues due to the inaccurate channel estimates of IAM, the time domain channel estimation techniques were proposed [13]–[20] . The authors in [13]–[18] propose time domain channel estimation techniques where guard symbols are required to separate different users' pilots. This leads to a spectral efficiency loss and limitations in terms of latency, especially as the number of users increases. Hence, clearly, in multiuser scenarios, reducing the pilot overhead for channel estimation becomes highly important. An alternative time domain channel estimation method for FBMC and its extension to MIMO channels was proposed in [19]. This method considers sending pilots for each antenna/user on all the subcarriers where the users' pilots are multiplexed in the code domain. This allows sharing the same time-frequency resources for channel estimation. The author also discusses a method of choosing a set of optimized codes in order to minimize the MSE of the estimated channels. Nevertheless, as [19] is not intended to cope with a muti-user scenario, and for the sake of minimizing the pilot overhead, there is only one FBMC pilot symbol per antenna (or user). In a multi-user context, this might limit the number of users that can be served. This time slot will be followed by one or more null FBMC symbols that act as a guard interval. This method is further studied in [20] where the associated formulations for the MMSE estimator and the Cramer-Rao lower bound are presented. Another interesting approach that has recently emerged in the literature is based on the idea of deploying a super imposed preamble with the data symbols, [21], [22]. In this approach, no isolation between the preamble and data symbols is required. While superimposed pilots

improve spectral efficiency, they require iterative interference cancellation. This process purifies the training signal from intrinsic interference coming from the data symbols at the expense of additional computational load.

To address the aforementioned issues for channel estimation and meet the stringent latency requirements of future networks, in this paper, we propose a pilot structure and a time domain channel estimation method for FBMC-based massive MIMO. Opposed to the existing literature, e.g., [23], our proposed pilot structure interleaves different users' pilots in time and frequency *without any guard symbols between them*, see Fig. 1. Furthermore, time domain channel estimation allows us to use as few as L pilots for channel estimation [24]. This clearly leads to a great amount of savings in signaling overhead. This, in turn, translates into a reduced latency and improved spectral efficiency, especially as the number of users increases. Furthermore, this brings a significant relaxation on the pilot contamination problem in massive MIMO networks, [25], given that the minimum number of pilots is assigned to each user. The proposed channel estimator takes advantage of the intrinsic interference due to the absence of guard symbols between different users' pilots and jointly estimates all the users' channel impulse responses. We also mathematically analyze our proposed channel estimator and obtain the statistics of the channel estimation errors, which prove to be useful in combatting the imperfect CSI effect.

Literature on multiple antenna FBMC receivers is mainly focused on MIMO-FBMC [13], [26]–[28]. References [26] and [13] propose approaches based on multi-tap fractionally spaced equalizer (FSE) for a MIMO setup. Authors in [26] use the frequency sampling (FS) approach to calculate per-subchannel equalizers. In [13], the authors use SINR and signal to leakage ratio as metrics to be maximized in designing multi-tap processing coefficients at the transmitter and receiver. Reference [28] proposes a tensor-based semi-blind approach for joint channel estimation and data detection in MIMO-FBMC systems. The identifiability of the canonical polyadic decomposition model introduced in [28] for MIMO-FBMC systems is not guaranteed. Interested readers are encouraged to refer to [29] for more details on channel estimation and equalization of FBMC systems.

In this paper, we address the channel equalization problem in FBMC-based massive MIMO, more inclined towards practical scenarios with both co-located and distributed antenna setups, i.e., cell-free MIMO [30]. In particular, we note that method of [6] where perfect knowledge of the underlying channel PDP is assumed at the receiver is not realistic. Hence, we develop new methods that operate based on channel estimates.

To summarize, the main contributions of this paper are the following; (1) We propose a joint multiuser and spectrally efficient channel estimation technique for the uplink of FBMC-based networks that is applicable to massive MIMO with both co-located and distributed antennas. We also derive the required statistics of the channel estimation errors to be used for their compensation at the equalization stage; (2) We investigate the channel equalization problem in FBMC-based massive MIMO and propose a practical two-stage equalization tech-

nique that is highly effective in both co-located and distributed antenna architectures; (3) We take into account the equalizer length in the design procedure to achieve an equalizer with a practical length; (4) We integrate the PDP estimates of the channel into our equalizer design framework and propose a practical PDP-based equalizer with a practical/short length; (5) We formulate FBMC-based cell-free massive MIMO for the first time and investigate channel estimation and equalization in this setup; (6) We derive the statistical characteristics of the estimation errors of our proposed channel estimator and incorporate them into our proposed equalizers to tackle the imperfect CSI effects.

The rest of the paper is organized as follows. Section II presents FBMC principles, paving the way towards presenting our proposed pilot structure and multiuser massive MIMO channel estimation technique in Section III. In Section IV, the principles of FBMC for massive MIMO are explained along with an asymptotic analysis that sheds light on the need for an extra stage of equalization after resolving the multiuser interference and a coarse equalization of the channel in the first stage. We show that this equalizer should be a fractionally spaced one and should be designed separately for each user. Two design techniques for the equalizers are also proposed. Section V expands our analysis to the imperfect CSI and discusses the corresponding equalizers. Section VI provides numerical analysis, confirming the validity of our claims through simulations. Finally, the paper is concluded in Section VII.

Notations: Matrices, vectors and scalar quantities are denoted by boldface uppercase, boldface lowercase and normal letters, respectively. $A(m, l)$ represents the element in the mth row and the lth column of $\mathbf{A}$ and $\mathbf{A}^{-1}$ signifies the inverse of $\mathbf{A}$. $\mathbf{I}_M$ is the identity matrix of size $M \times M$, and $\mathbf{D} = \text{diag}(\mathbf{a})$ is a diagonal matrix with diagonal elements in the vector $\mathbf{a}$. Superscripts $(\cdot)^{-1}$, $(\cdot)^{\text{T}}$, $(\cdot)^{\text{H}}$ and $(\cdot)^*$ indicate inverse, transpose, conjugate transpose, and conjugate operations, respectively. $\Re\{\cdot\}$, $\Im\{\cdot\}$, $\mathbb{E}\{\cdot\}$, $(\downarrow M)$, $\star$ and $\text{tr}\{\cdot\}$ represent real value, imaginary value, expectation, M fold decimation, linear convolution and matrix trace operators, respectively. Operator $\mathcal{T}_{M \times N}(\mathbf{a})$ transforms the vector $\mathbf{a}$ into a $M \times N$ Toeplitz matrix. Finally, δ_{ij} represents the Kronecker delta function.

II. FBMC PRINCIPLES

We consider the discrete time baseband equivalent of the staggered multi-tone (SMT) system. This modulation scheme divides the transmission bandwidth into M sub-carrier bands with the normalized bandwidth of $1/M$ each. The real-valued data symbols in SMT are placed on a regular time-frequency grid with the time and frequency spacings of $T/2$ and $1/T$, respectively. Thus, the synthesized signal is expressed as

$$x[l] = \sum_{m=0}^{M-1} \sum_{n=-\infty}^{\infty} s_{m,n} f_{m,n}[l], \qquad (1)$$

where $s_{m,n}$ is the real-valued data symbol at the frequency index m and the time index n, and

$$f_{m,n}[l] = f\left[l - n\frac{M}{2}\right] e^{j2\pi ml/M} e^{j\pi(m+n)/2}, \qquad (2)$$

is the modulated and phase-adjusted pulse-shape that carries $s_{m,n}$.

In (2), $f[l]$ is a prototype filter that is designed such that for all pairs of (m, n) and (m', n')

$$\Re\left\{ \sum_{l=-\infty}^{\infty} f_{m,n}[l] f_{m',n'}^*[l] \right\} = \delta_{mm'}\delta_{nn'}. \qquad (3)$$

This property, which is known as orthogonality in the real field, implies that the set of functions $f_{m,n}[l]$, for all choices of m and n, defines a basis set that carries the real-valued data symbols $s_{m,n}$. These data symbols can be extracted from the synthesized signal $x[l]$ by projecting $x[l]$ on the basis functions $f_{m,n}[l]$ and taking the real-part of the results. That is,

$$s_{m,n} = \Re\left\{ \langle x[l], f_{m,n}[l] \rangle \right\}, \qquad (4)$$

and projection of $x[l]$ on $f_{m,n}[l]$ is defined as

$$\langle x[l], f_{m,n}[l] \rangle = \sum_{l=-\infty}^{\infty} x[l] f_{m,n}^*[l]. \qquad (5)$$

Assuming a time-invariant channel, the received signal at the receiver can be written as

$$r[l] = h[l] \star x[l] + \eta[l], \qquad (6)$$

where $h[l]$ represents multi-path channel impulse response with length L and $\eta[l]$ is additive white Gaussian noise (AWGN) with the variance of σ_η^2, i.e., $\eta[l] \sim \mathcal{CN}(0, \sigma_\eta^2)$.

We define the analyzed/demodulated signal samples

$$z_{m,n} = \langle r[l], f_{m,n}[l] \rangle, \qquad (7)$$

and note that the data symbols $s_{m,n}$ are extracted by passing the sequence $z_{m,n}$ through an equalizer and taking the real-part of the output. In its simplest form, when the channel is approximated by a flat gain across each subcarrier band, a single-tap equalizer is sufficient. Since this approximation is not always valid, a multi-tap equalizer may be favorable, [31]. For the equalizer to provide a satisfactory performance, accurate channel estimation is of a paramount importance. Thus, the following section is focused on channel estimation.

III. CHANNEL ESTIMATION

In this section, we propose a spectrally efficient pilot structure and a joint multiuser channel estimation technique for the uplink of FBMC-based networks. We also provide the estimation error characteristics of the proposed method. This will be used in the following sections to mitigate the imperfect CSI effects on the proposed channel equalization techniques. In our proposed channel estimation method, we use only L rather than M pilot subcarriers per user. Noting that typically $L \ll M$, using L pilots significantly reduces the signaling overhead. Moreover, to further reduce the signaling overhead, guard bands are avoided between different users' pilot subcarriers. However, to avoid interference between the pilot and data symbols, we follow the previous literature, [16], and insert a few guard symbols after pilot symbols. The proposed pilot structure is presented in Fig. 1.

As we perform per antenna channel estimation, for the sake of simplicity of the notations and without loss of generality,
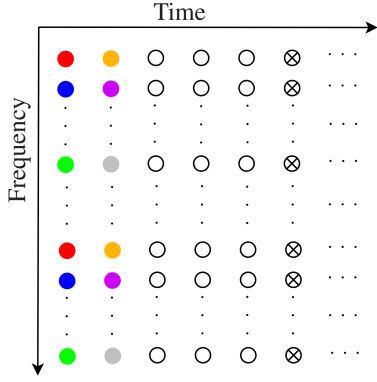
Fig. 1. Proposed pilot structure for channel estimation in the uplink. Different users' pilots are specified with different colors. Crossed circles and empty circles represent data and zero symbols, respectively.

we drop the antenna index. We assume that K users transmit their pilot symbols simultaneously. The pilot symbols that are transmitted by the kth user are put together in the real-valued column vector $\mathbf{p}_k = [p_0^k, p_1^k, \ldots, p_{N_p-1}^k]^T$, where we assume equal number of pilots, N_p, for all the users and the associated demodulated vector at the receiver is the complex-valued column vector and $\mathbf{z}_k = [z_{p_0^k}, z_{p_1^k}, \ldots, z_{p_{N_p-1}^k}]^T$.

Following the SMT signal synthesis in (1) and signal analysis in (7), and straightforward manipulations lead to, [32],

$$\bar{\mathbf{z}} = \bar{\mathbf{A}}\bar{\mathbf{h}} + \bar{\boldsymbol{\eta}}, \qquad (8)$$

where $\bar{\mathbf{z}} = [\mathbf{z}_0^T, \ldots, \mathbf{z}_{K-1}^T]^T$, $\bar{\mathbf{h}} = [\mathbf{h}_0^T, \ldots, \mathbf{h}_{K-1}^T]^T$, $\bar{\boldsymbol{\eta}} = [\boldsymbol{\eta}_0^T, \ldots, \boldsymbol{\eta}_{K-1}^T]^T$, $\mathbf{h}_k = [h_k[0], \ldots, h_k[L-1]]^T$ is the channel vector of user k, $\boldsymbol{\eta}_k$ is the noise contribution to the received pilot sequence of user k, and

$$\bar{\mathbf{A}} = \begin{bmatrix} \mathbf{A}_0 & \boldsymbol{\zeta}_0^1 & \cdots & \boldsymbol{\zeta}_0^{K-1} \\ \boldsymbol{\zeta}_1^0 & \mathbf{A}_1 & \cdots & \boldsymbol{\zeta}_1^{K-1} \\ \vdots & \vdots & \ddots & \vdots \\ \boldsymbol{\zeta}_{K-1}^0 & \boldsymbol{\zeta}_{K-1}^1 & \cdots & \mathbf{A}_{K-1} \end{bmatrix}. \qquad (9)$$

The matrices $\mathbf{A}_k$ and $\boldsymbol{\zeta}_{k_1}^{k_2}$ are of size $N_p^k \times L$ and $N_p^{k_1} \times L$, respectively, and have the elements

$$A_k(i,\iota) = \sum_q \sum_{m'} \sum_{n'} s_{m',n'}^k f[q - \iota - n'\tfrac{M}{2}] f[q - n_i^k \tfrac{M}{2}]$$
$$\times e^{j\frac{2\pi(m'-m_i^k)q}{M}} e^{j\frac{\pi(m'+n'-m_i^k-n_i^k)}{2}} e^{-j\frac{2\pi m'\iota}{M}}, \qquad (10)$$

and

$$\zeta_{k_1}^{k_2}(i,\iota) = \sum_q \sum_{m'} \sum_{n'} s_{m',n'}^{k_2} f[q - \iota - n'\tfrac{M}{2}] f[q - n_i^{k_1}\tfrac{M}{2}]$$
$$\times e^{j\frac{2\pi(m'-m_i^{k_1})q}{M}} e^{j\frac{\pi(m'+n'-m_i^{k_1}-n_i^{k_1})}{2}} e^{-j\frac{2\pi m'\iota}{M}}, \quad (11)$$

where (m_i^k, n_i^k) is the pair of time-frequency indices that map to the ith row of $\mathbf{A}_k$. We may also note that the columns of $\mathbf{A}_k$ are aligned with the sample position in the respective channel impulse response $\mathbf{h}_k$.

The matrix $\mathbf{A}_k$ is the gain factor indicating the contribution of pilots transmitted by the user k on the respective demodulated signals at the receiver. The matrix $\boldsymbol{\zeta}_{k_1}^{k_2}$, on the other hand,

indicates the intrinsic interference produced by the pilots of the user k_2 on the demodulated signals of the user k_1. Hence, (8) decouples the users' channel responses from their training sequences. This enables accurate estimation of all the users' channel impulse responses by taking into account the intrinsic interference between the users' pilot sequences.

We also note that overlapping of the subcarrier bands in SMT introduces some correlation among the elements of the noise vector $\bar{\boldsymbol{\eta}}$. These correlations lead to a covariance matrix $\mathbf{C}_{\bar{\eta}\bar{\eta}}$ whose impact on the minimum variance unbiased (MVU) estimate of $\bar{\mathbf{h}}$ is reflected in the following equation, [33],

$$\hat{\bar{\mathbf{h}}} = (\bar{\mathbf{A}}^H \mathbf{C}_{\bar{\eta}\bar{\eta}}^{-1} \bar{\mathbf{A}})^{-1} \bar{\mathbf{A}}^H \mathbf{C}_{\bar{\eta}\bar{\eta}}^{-1} \bar{\mathbf{z}}. \qquad (12)$$

The (i,j)th element of the covariance matrix $\mathbf{C}_{\bar{\eta}\bar{\eta}}$ may be calculated as

$$\begin{aligned} C_{\bar{\eta}\bar{\eta}}(i,j) &= \mathrm{cov}[\eta_{m_i,n_i}, \eta_{m_j,n_j}] \\ &= \mathbb{E}[\eta_{m_i,n_i}\eta_{m_j,n_j}^*] - \mathbb{E}[\eta_{m_i,n_i}]\mathbb{E}[\eta_{m_j,n_j}^*] \\ &= \sigma_\eta^2 \sum_{l=-\infty}^{\infty} f[l]f^*[l] e^{j\frac{2\pi(m_j-m_i)l}{M}} e^{j\frac{\pi(m_j+n_j-m_i-n_i)}{2}}, \end{aligned} \qquad (13)$$

where σ_η^2 is the noise variance at the receiver input, and the pairs of (m_i, n_i) and (m_j, n_j) are the pairs of time-frequency indices that map to the ith and jth elements of $\bar{\boldsymbol{\eta}}$. The structure of this matrix is related to the order of the pilots assigned to the users which forms the order of the pilots used in the concatenated vector $\bar{\boldsymbol{\eta}}$.

It is further noted that the presence of channel noise leads to inaccurate channel estimates $\hat{\bar{\mathbf{h}}}$. This adversely affects signal detection. Hence, it is of a great importance to take the noise characteristics into account at the detection stage. Based on the results from estimation theory, [33], the channel estimation MSE can be found as

$$\mathrm{MSE} = \mathrm{tr}\{(\bar{\mathbf{A}}^H \mathbf{C}_{\bar{\eta}\bar{\eta}}^{-1} \bar{\mathbf{A}})^{-1}\}. \qquad (14)$$

This, in part, depends on pilot sets and prototype filter, hence, can be pre-calculated off-line. There is also a proportionality constant equal to the channel noise power that may be added on-line.

For ease of derivations, we approximate the error variance for all the taps of all the users' channel estimates to be equal to the average estimation error. Accordingly, the estimation error for the channel tap l between BS antenna i and user k, $\Delta h_{i,k}[l]$, may be approximated by a complex Gaussian distribution with zero mean and the variance

$$\sigma_{\mathrm{et}}^2 = \frac{\mathrm{MSE}}{K \times L}. \qquad (15)$$

The accuracy of this approximation has been confirmed through extensive empirical experiments. The simulation results that are presented in Section VI also confirm that this is a fair approximation.

Our proposed equalization techniques in the following section require the statistics of the estimation errors in the frequency domain. Using Parseval's theorem, one may realize

that estimation error at a given subcarrier m, also follows complex Gaussian distribution with the variance

$$\sigma_{\text{ef}}^2 = L\sigma_{\text{et}}^2. \qquad (16)$$

That is, $\Delta H_m^{i,k} \sim \mathcal{CN}(0, \sigma_{\text{ef}}^2)$.

It may be further noted that the limited length of the channel response in the time-domain implies that the estimation errors $\Delta H_m^{i,k}$, across different subcarriers, are not independent. Nevertheless, since in this paper, signals from different subcarriers are processed independently, such correlation has no relevant impact on our receiver design and thus is ignored in the rest of our discussions.

IV. MASSIVE MIMO FBMC: ASYMPTOTIC ANALYSIS AND EQUALIZER DESIGN

In this section, we develop practical channel equalization techniques for FBMC-based massive MIMO with co-located and distributed antennas. To this end, we start with modifying the existing PDP equalizer in [6] and propose an equalizer shortening method that leads to a substantially reduced delay. This, in particular, makes our proposal attractive for applications with stringent latency requirements. We also take note that the PDP equalizer of [6] relies on the assumption that the number of BS antennas is large. We propose a per-subcarrier equivalent channel-based equalization technique that does not rely on this assumption. This new design will be found instrumental in cell-free networks where the number of effective antennas seen by each user terminal remains small and the channel PDPs vary among different receiver antennas. The proposed equivalent channel-based FSE also sets a benchmark for evaluating the performance of the PDP equalizer of [6] and its modified version here.

Let us consider a single-cell massive MIMO setup including a BS equipped with N antennas and K single-antenna users. The received signal at a given antenna i can be expressed as

$$r_i[l] = \sum_{k=0}^{K-1} x_k[l] \star h_{i,k}[l] + \eta_i[l], \qquad (17)$$

where $x_k[l]$ is user k transmit signal, $\eta_i[l] \sim \mathcal{CN}(0, \sigma_\eta^2)$ is the additive noise at BS antenna i and $h_{i,k}[l]$ is the channel impulse response between user k and BS antenna i. We assume that the BS antenna array is sufficiently compact and model the channels between any given user k and all the BS antennas with the same PDP, i.e., $p_k[\ell]$ for $\ell = 0, \ldots, L-1$. Thus, the channel taps $h_{i,k}[\ell]$ follow the distribution $\mathcal{CN}(0, p_k[\ell])$ and are independent of one another. Furthermore, we assume the average transmit power of unity for each user terminal.

Stacking the demodulated signals corresponding to different BS antennas, after phase adjustment (i.e., removing the phase factor $e^{j\pi(m+n)/2}$) but before taking the real part, into $N \times 1$ vectors $\mathbf{z}_{m,n}$, we have

$$\mathbf{z}_{m,n} = \sum_{n'=-\infty}^{+\infty} \sum_{m'=0}^{M-1} \mathbf{H}_{mm',nn'} \mathbf{s}_{m',n'} + \boldsymbol{\eta}_{m,n}, \qquad (18)$$

where the vector $\mathbf{s}_{m,n} = [s_{m,n}^0, \ldots, s_{m,n}^{K-1}]^{\text{T}}$ contains the real-valued data symbols of different users at the time-frequency slot (m,n), $\boldsymbol{\eta}_{m,n}$ is the contribution of noise, and $\mathbf{H}_{mm',nn'}$ is the $N \times K$ gain matrix among data symbols across both time and frequency with the elements of

$$H_{mm',nn'}^{i,k} = h_{mm'}^{i,k}[n - n']e^{j(m'+n'-m-n)\frac{\pi}{2}}, \qquad (19)$$

where $f_m[l] = f[l]e^{j2\pi ml/M}$ and $h_{mm'}^{i,k}[n] = \left(f_{m'}[l] \star h_{i,k}[l] \star f_m^*[l]\right)_{\downarrow\frac{M}{2}}$. Considering perfect synchronization and knowledge of the channel, and using a per-subcarrier combiner matrix $\mathbf{W}_m$, the data symbols of different users are estimated as

$$\hat{\mathbf{s}}_{m,n} = \Re\{\mathbf{W}_m^{\text{H}} \mathbf{z}_{m,n}\}$$
$$= \Re\{\sum_{n'=-\infty}^{+\infty} \sum_{m'=0}^{M-1} \mathbf{G}_{mm',nn'} \mathbf{s}_{m',n'} + \boldsymbol{\eta}_{m,n}'\}, \qquad (20)$$

where $\mathbf{G}_{mm',nn'} = \mathbf{W}_m^{\text{H}} \mathbf{H}_{mm',nn'}$ and $\boldsymbol{\eta}_{m,n}' = \mathbf{W}_m^{\text{H}} \boldsymbol{\eta}_{m,n}$. The common linear combiners, the maximum ratio combining (MRC), the zero forcing (ZF) detector, and the minimum mean square error (MMSE) detector, are respectively defined as

$$\mathbf{W}_m = \begin{cases} \mathbf{H}_m \mathbf{D}_m^{-1}, & \text{for MRC}, \\ \mathbf{H}_m (\mathbf{H}_m^{\text{H}} \mathbf{H}_m)^{-1}, & \text{for ZF}, \\ \mathbf{H}_m (\mathbf{H}_m^{\text{H}} \mathbf{H}_m + \sigma_\eta^2 \mathbf{I}_K)^{-1}, & \text{for MMSE}, \end{cases} \qquad (21)$$

where $\mathbf{H}_m$ is the $N \times K$ channel matrix whose element, (i,k) represents the channel gain at the center of a given subcarrier m between user k and BS antenna i, i.e., $H_m^{i,k} \triangleq \sum_{l=0}^{L-1} h_{i,k}[l]e^{-j\frac{2\pi ml}{M}}$. In MRC, the $K \times K$ diagonal matrix $\mathbf{D}_m$ normalizes the combiner outputs with the coefficients $D_m^{k,k} = \sum_{i=0}^{N-1} |H_m^{i,k}|^2$.

The authors in [6] have shown that even with an infinite number of antennas, a residual interference remains at the output of any of the above combiners. It has been also noted that for a large number of antennas, all the above combiners converge to $\frac{1}{N}\mathbf{H}_m$, [34]. Accordingly, the equivalent channel impulse response between the transmitted symbols at subcarrier m' of terminal k' and the received and combined signal at subcarrier m of BS output corresponding to terminal k may be expressed as

$$g_{mm'}^{k,k'}[n] = \left(f_{m'}[l] \star h_{k,k',m}^{(\text{eqvlt})}[l] \star f_m^*[l]\right)_{\downarrow\frac{M}{2}}. \qquad (22)$$

where

$$h_{k,k',m}^{(\text{eqvlt})}[l] = \frac{1}{N} \sum_{i=0}^{N-1} (H_m^{i,k})^* h_{i,k'}[l], \qquad (23)$$

is the combined/equivalent channel between the user terminal k' and the combiner output of the kth user over the subcarrier band m.

In [6], it is shown that for a large number of antennas N, at the BS, $h_{k,k',m}^{(\text{eqvlt})}[l]$ vanishes to zero, when $k \neq k'$, and when $k = k'$, $h_{k,k,m}^{(\text{eqvlt})}[l]$ in (22) may be replaced by

$$\bar{p}_{m,k}[l] = p_k[l]e^{j2\pi lm/M}, \qquad (24)$$

where $p_k[l]$ is the channel PDP between the user terminal k and the BS antennas.

It has been further argued in [6] that the presence of $h_{k,k',m}^{(\text{eqvlt})}[l]$ (equivalently, $\bar{p}_{m,k}[l]\delta_{kk'}$) in (22) breaks the Nyquist

property between the transmit and receive prototype filters. Hence, a per subcarrier equalizer should be adopted to undo the effect of $h_{k,k',m}^{(\text{eqvlt})}[l]$. Accordingly, [6] has proposed the zero forcing equalizer

$$\Phi_{m,k}(\omega) = 1/\bar{P}_{m,k}(\omega), \tag{25}$$

where $\bar{P}_{m,k}(\omega)$ is the discrete-time Fourier transform (DTFT) of $\bar{p}_{m,k}[l]$.

The rest of this section is organized as follows. We first revisit the PDP-based equalizer design of [6], take note that it is only applicable to large and co-located antenna systems, mention some of the inherent problems of this design, and propose a new design technique for resolving these problems. Next, we note that in distributed antenna systems, where the antennas that are attached to a BS are distributed over a wide area for a higher diversity gain, [30], the underlying channels have different PDPs and thus the PDP equalizer design is not applicable. The same is true for cell-free MIMO systems [35]. Moreover, we note that when the number of BS antennas is small, the PDP equalizer may not be effective. We thus propose a new equalizer design that can serve these scenarios. Lastly, we take note that the distributed antenna/cell-free systems need a special treatment to keep the same fairness for all users in the network.

A. Large and co-located antenna systems

Further study of the above equalizer design reveals that, [6], the equalizer (25) may be implemented at baseband, i.e., after the analysis filter bank, the $M/2$-fold decimation, and the combining (20), but before taking the real-part. This, obviously, reduces the complexity of the receiver significantly as the equalizer is implemented at a reduced sampling rate. The implemented equalizer in the baseband is the demodulated and $M/2$-fold decimated version of $\Phi_{m,k}(\omega)$, in the time domain. Furthermore, the demodulated version of $\Phi_{m,k}(\omega)$, i.e., $\Phi_{0,k}(\omega)$, before decimation has to be band limited through an antialiasing filter. Another point that needs to be noted is that the baseband equalizer designed here is an FSE [36] with tap-spacing of half symbol spacing. A detailed derivation of a PDP-based FSE based on MMSE criterion is provided in Appendix A. This design approach can be used for the equivalent channel-based FSE as well.

In typical FBMC systems, the prototype filter is often chosen to be a square-root Nyquist filter with an excess bandwidth of 100%, equivalent to a roll-off factor $\alpha = 1$. This leaves no room for the transition band of the antialiasing filter that was mentioned above. Hence, [6] has proposed the use of a brick-wall antialiasing filter. Such brick-wall filter, unfortunately, increases the length of the equalizer significantly. This leads to both complexity and latency issues. Here, we propose a modified design that solves these shortcomings of the PDP equalizer design of [6].

We first note that for $k = k'$ and $m = m'$, replacement of (24) in (22) leads to

$$g_{mm}^{k,k}[n] = \left(f_m[l] \star p_k[l] e^{j2\pi lm/M} \star f_m^*[l]\right)_{\downarrow \frac{M}{2}}. \tag{26}$$

Noting that $f_m[l]$ is a bandpass filter with a bandwidth of $2/M$, centered at the subcarrier frequency $f_c = 1/M$, and

following the basic theory of multirate signal processing [37], [38], it is straightforward to show that $g_{mm}^{k,k}[n]$ is a baseband signal that spans over the frequency band $-\frac{1}{M} < f < \frac{1}{M}$. It is also known that the decimation by $M/2$ may be viewed as a demodulation process that removes the modulation factor $e^{j2\pi lm/M}$ from all the terms on the right-hand side of (26), leading to

$$g_k[n] = \left(f[l] \star p_k[l] \star f[l]\right)_{\downarrow \frac{M}{2}}, \tag{27}$$

where we have defined the pulse-shape $g_k[n] = g_{mm}^{k,k}[n]$. , noting that the right-hand side of (27) is independent of m.

The result in (27) shows that a common equalizer that removes any inter-symbol interference (ISI) generated by the pulse-shape $g_k[n]$ may be designed and applied to all subcarrier signals at the FBMC receiver output, i.e., after analysis filter bank, decimation, and combining. This equalizer is a fractionally spaced one, [37], [39], that, for any m, covers the m-th band of the filter bank, including the portions of the band that overlap with the adjacent bands. It thus also removes the intrinsic interference from the adjacent bands. The equalizer design, here, may be a ZF or an MMSE one that can provide a satisfactory performance with a very small number of taps. As a result, our proposal here addresses the aforementioned complexity and latency issues of the equalizer in [6]. Numerical examples that show the impact of these modifications on the design of the equalizer, when compared to equalizer design of [6], are discussed in Section VI.

B. Small antenna systems

We first note that when the number of BS antennas is small, the ZF or MMSE combiners significantly outperform MRC, hence, should be adopted. When any of these combiners is adopted, the equivalent channel response (23), for $k = k'$, should be replaced by

$$h_{k,k,m}^{(\text{eqvlt})}[l] = \sum_{i=0}^{N-1} (W_m^{i,k})^* h_{i,k}[l], \tag{28}$$

where the coefficients $W_m^{i,k}$ are the combiner coefficients given by the ZF or MMSE combiner in (21). Substituting (28) in (22) leads to

$$g_{mm}^{k,k}[n] = \left[f_m[l] \star \left(\sum_{i=0}^{N-1} (W_m^{i,k})^* h_{i,k}[l]\right) \star f_m^*[l]\right]_{\downarrow \frac{M}{2}}. \tag{29}$$

Following the discussions surrounding equations (26) and (27), above, one will find that, here, $g_{mm}^{k,k}[n]$ is a baseband pulse-shape that, unlike $g_k[n]$ in (27), varies with the subcarrier index m. Hence, here, for each subcarrier band, we propose designing a ZF or MMSE equalizer that removes ISI in the pulse-shape $g_{mm}^{k,k}[n]$ of (29). The numerical results that are presented in Section VI show an excellent performance of this design. In particular, we find that even for a small number of BS antennas, when this equalizer design is applied to the output of a ZF or MMSE combiner, the receiver performance remains very similar to that of the single user performance. This observation may be explained as follows. The ZF or MMSE combiner removes most of the multi-user interference.
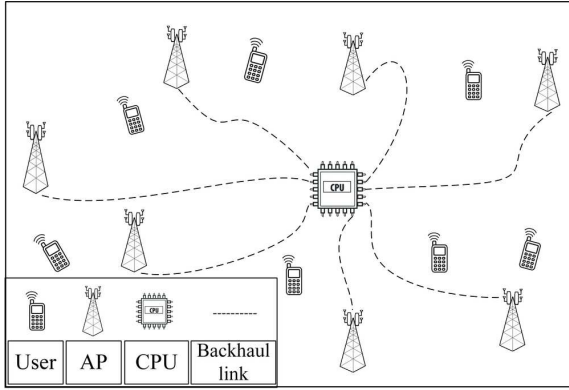
Fig. 2. Cell-free massive MIMO network architecture.

The remaining distortion, which is limited to the user of interest, is then removed by the equalizer.

C. Cell-free/distributed antenna systems

In this scenario, N_{AP} distributed access points (APs) are connected to a central processing unit (CPU) through a backhaul network as in Fig 2. We consider a centralized processing scenario in the uplink, similar to [35], where the CPU performs detection by processing all the received signals from N total antennas. It is worth mentioning that distinct APs are assigned antenna indices that belong to mutually disjoint subsets of the available antennas, i.e., a given antenna is only assigned to one AP. In this work, without loss of generality, we consider APs that are equipped with an equal number of antennas, i.e., $\frac{N}{N_{AP}}$ antennas each.

In the previous cases, we assumed perfect power control. Hence, we assumed the normalized PDP which would result in $\sum_l p_{i,k}[l] = 1$, for all pairs of i and k. In a cell-free/distributed antenna scenario, $\sum_l p_{i,k}[l] = \beta_{i,k}$, where $\beta_{i,k}$ is a large-scale fading coefficient that depends on the distance between a given user k and an antenna i and any shadowing effects, [30], [40]. We assume the same normalized PDP and the large-scale fading coefficient for a given user and all the antennas of a given AP.

The presence of different large-scale fading coefficients with large variations between a given user and APs in a cell-free massive MIMO architecture results in fairness issues [30]. This necessitates the application of effective power control methods that can strike a balance between fairness and average SINR performance [41]. Hence, here, we deploy the fractional power control that is proposed for OFDM-based cell-free massive MIMO in [42]. This is an extended form of the power control method used in the long term evolution (LTE) standard. Based on the results of [42], the power control coefficient for a given user k in the uplink of a cell-free massive MIMO can be obtained as

$$\mu_k \propto \frac{1}{\left(\sum_{i=0}^{N-1} \beta_{i,k}\right)^{\nu}}. \tag{30}$$

where ν is a design parameter to be set between 0.5 and 0.7, [41], [43]. By changing ν, we are able to adjust the trade-off

between fairness and average SINR. Thus, the transmit signal of user k may be expressed as

$$x_k[l] = \sum_{m=0}^{M-1} \sum_{n=-\infty}^{\infty} \sqrt{\mu_k} s_{m,n}^k f_{m,n}[l]. \tag{31}$$

This is a simple modification to (1) which leads to the following modified form of the equivalent channel (28).

$$h_{k,k,m}^{(\text{eqvlt})}[l] = \sum_{i=0}^{N-1} (W_m^{i,k})^* \sqrt{\mu_k} h_{i,k}[l]. \tag{32}$$

The FSE design thus follows accordingly.

D. Summary

Fig. 3 summarizes our proposal in this section as a two-stage equalization process following the analysis filter bank (AFB) steps expressed by (18) and (19). The first stage is a conventional linear combining that equalizes the channels at the center of the subcarrier bands and separates different users' signals. This stage can be thought of as a coarse equalization and multiuser detection stage. In the second stage, the output of the first stage is passed through a set of FSEs that repeat for each subcarrier m and every user k for removal of any residual ISI as well as any inter-carrier interference (ICI).

V. CHANNEL EQUALIZATION WITH IMPERFECT CSI

The equalizer designs that have been proposed so far are based on the assumption of having perfect CSI at all the BS antennas. Obviously, in practical systems, the presence of channel estimation errors can adversely affect the performance of these equalizers. Here, we use the results of Section III and modify our proposed designs in Section IV to take the statistics of the channel estimation errors into account in the detection stage.

A. Large and co-located antenna systems

The combiners with imperfect CSI are derived by substituting $H_m^{i,k}$ with $\hat{H}_m^{i,k} = H_m^{i,k} + \Delta H_m^{i,k}$ in (21). Here, to get some insight, we look at these combiners by exploring their performance in the asymptotic regime where N grows to a large value.

We recall that, in the case of MRC, $\mathbf{D}_m$ is a diagonal matrix with the diagonal elements $D_m^{k,k} = \sum_{i=0}^{N-1} |H_m^{i,k}|^2$. With imperfect CSI, this becomes

$$\hat{D}_m^{k,k} = \sum_{i=0}^{N-1} |H_m^{i,k} + \Delta H_m^{i,k}|^2. \tag{33}$$

Assuming uncorrelated estimation errors and channel gains, by the law of large numbers, in the asymptotic regime, $\hat{D}_m^{k,k}$ converges to

$$N\mathbb{E}\{|H_m^{i,k}|^2\} + N\mathbb{E}\{|\Delta H_m^{i,k}|^2\} = N + N\sigma_{\text{ef}}^2. \tag{34}$$

Using a similar approach for the ZF combiner, it is not hard to show that in the asymptotic regime $\hat{\mathbf{H}}_m^H \hat{\mathbf{H}}_m$ converges to $\hat{\mathbf{D}}_m$. Hence, the ZF combiner performance loss due to channel estimation error follows that of the MRC.
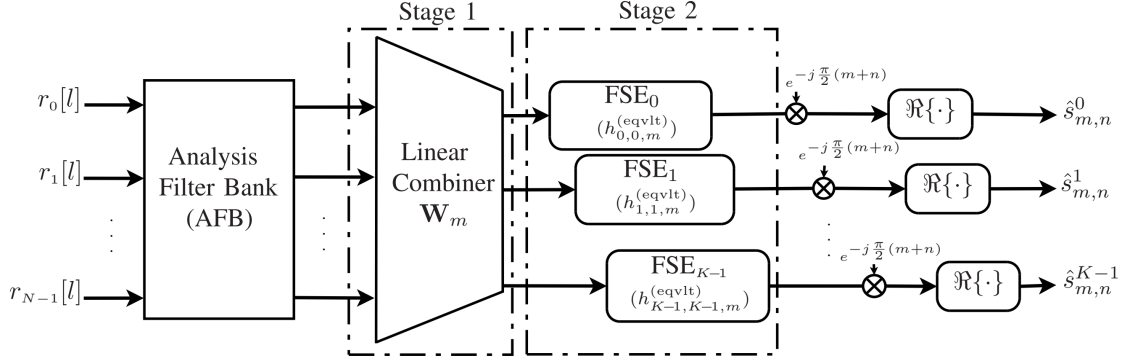
Fig. 3. The proposed two-stage equalization receiver structure. The first stage is a conventional linear combining that equalizes the channels at the center of the subcarrier bands and separates different users' signals. At the second stage, the output of the first stage is passed through a set of FSEs that repeat for a given subcarrier m and a given user k for removal of any residual ISI and ICI.

In the MMSE combiner case, we argue that as N grows large, σ_η^2 will become negligible when compared to $N + N\sigma_{\text{ef}}^2$ and, hence, MMSE combiner will converge to the ZF combiner which in the asymptotic regime is similar to the MRC. These show that in the asymptotic regime, all three combiners converge to $\hat{\mathbf{W}}_m = \frac{1}{N(1+\sigma_{\text{ef}}^2)}\hat{\mathbf{H}}_m$. Consequently, from (20), the combined/equivalent channel between the transmit symbol at subcarrier m' of terminal k' and the received one at subcarrier m, at the kth combiner output converges to

$$h_{k,k',m}^{(\text{eqvlt})}[l] = \frac{1}{N(1+\sigma_{\text{ef}}^2)}\sum_{i=0}^{N-1}(\hat{H}_m^{i,k})^* h_{i,k'}[l]. \quad (35)$$

Moreover, for large values of N, (35), reduces to

$$h_{k,k',m}^{(\text{eqvlt})}[l] = \frac{1}{1+\sigma_{\text{ef}}^2}\mathbb{E}\{(\hat{H}_m^{i,k})^* h_{i,k'}[l]\}. \quad (36)$$

Assuming independent channel responses for different users, independent channel taps, and uncorrelated channel estimation errors, one will find that

$$\mathbb{E}[(\hat{H}_m^{i,k})^* h_{i,k'}[l]] = p_k[l]e^{j2\pi lm/M}\delta_{kk'}. \quad (37)$$

Thus, the equivalent channel converges to

$$h_{k,k',m}^{(\text{eqvlt})}[l] = \tilde{p}_{m,k}[l]\delta_{kk'}, \quad (38)$$

where

$$\tilde{p}_{m,k}[l] = \frac{\bar{p}_{m,k}[l]}{1+\sigma_{\text{ef}}^2}. \quad (39)$$

The above results lead to the following conclusion. To compensate for the imperfect CSI, the scaling factor $1/(1+\sigma_{\text{ef}}^2)$ should be added to the PDP $\bar{p}_{m,k}[l]$. This is equivalent to adding the *correction factor* $1+\sigma_{\text{ef}}^2$ to the designed equalizer. The accuracy of this modified design is corroborated through simulations in Section VI.

PDP approximation: In the imperfect CSI scenario, the knowledge of channel statistics is not always available. Thus, we propose to approximate the PDP by taking the average

$$\hat{p}_k[l] = \frac{1}{N}\sum_{i=0}^{N-1}|\hat{h}_{i,k}[l]|^2. \quad (40)$$

This is then replaced for $p_k[l]$ in (37).

B. Small antenna systems

Substituting the channel estimates in (28), we obtain the equivalent channel estimate

$$\hat{h}_{k,k',m}^{(\text{eqvlt})}[l] = \sum_{i=0}^{N-1}(\hat{W}_m^{i,k})^* \hat{h}_{i,k'}[l], \quad (41)$$

where $\hat{h}_{i,k'}[l] = h_{i,k'}[l] + \Delta h_{i,k'}[l]$.

Here, for moderate and large values of N,

$$\hat{h}_{k,k',m}^{(\text{eqvlt})}[l] \to \frac{1}{1+\sigma_{\text{ef}}^2}\mathbb{E}\{(\hat{H}_m^{i,k})^* \hat{h}_{i,k'}[l]\}. \quad (42)$$

Assuming independent channel responses and uncorrelated estimation errors,

$$\begin{aligned}
\mathbb{E}\{(\hat{H}_m^{i,k})^* \hat{h}_{i,k'}[l]\} &= \sum_{l'=0}^{L-1}\mathbb{E}\{h_{i,k'}^*[l']h_{i,k}[l]\}e^{j2\pi l'm/M} \\
&\quad + \sum_{l'=0}^{L-1}\mathbb{E}\{\Delta h_{i,k}^*[l']\Delta h_{i,k'}[l]\}e^{j2\pi l'm/M} \\
&= \bar{p}_{m,k}[l]\delta_{kk'} + \sigma_{\text{et}}^2 e^{j2\pi lm/M}\delta_{kk'}.
\end{aligned} \quad (43)$$

Hence, (42) can be written as

$$\hat{h}_{k,k',m}^{(\text{eqvlt})}[l] \to h_{k,k',m}^{(\text{eqvlt})}[l] + \frac{\sigma_{\text{et}}^2 \delta_{kk'}}{1+\sigma_{\text{ef}}^2}e^{j2\pi lm/M}. \quad (44)$$

where the second term on the right-hand side of (44) is due to the effect of channel estimation errors. This can be simply mitigated by subtracting the *correction term* $\frac{\sigma_{\text{et}}^2 \delta_{kk'}}{1+\sigma_{\text{ef}}^2}e^{j2\pi lm/M}$ from the equivalent channel estimate (41) and designing the equalizer based on the modified channel estimate. The efficacy of this solution is corroborated by simulations in Section VI.

C. Cell-free/distributed antenna systems

Here, (41) is replaced by

$$\hat{h}_{k,k',m}^{(\text{eqvlt})}[l] = \sum_{i=0}^{N-1}(\hat{W}_m^{i,k})^* \sqrt{\mu_k}\hat{h}_{i,k'}[l], \quad (45)$$

Following the same line of derivations as in [34], as the number of antennas, N, grows large, here, the combiners converge to $\mathbf{W}_m = \mathrm{diag}([\sum_{i=0}^{N-1} \beta_{i,0}, ..., \sum_{i=0}^{N-1} \beta_{i,K-1}])^{-1} \mathbf{H}_m$. Hence,

$$\hat{h}_{k,k',m}^{(\text{eqvlt})}[l] \to \frac{\sqrt{\mu_k}}{\sum_{i=0}^{N-1} \beta_{i,k} + N\sigma_{\text{ef}}^2} \sum_{i=0}^{N-1} \mathbb{E}\big\{(\hat{H}_m^{i,k})^* \hat{h}_{i,k'}[l]\big\}. \tag{46}$$

Also, assuming independent channel responses and uncorrelated estimation errors, one will find that

$$\mathbb{E}\big\{(\hat{H}_m^{i,k})^* \hat{h}_{i,k'}[l]\big\} = \sum_{l'=0}^{L-1} \mathbb{E}\big\{h_{i,k'}^*[l']h_{i,k}[l]\big\}e^{j2\pi l'm/M}$$
$$+ \sum_{l'=0}^{L-1} \mathbb{E}\big\{\Delta h_{i,k}^*[l']\Delta h_{i,k'}[l]\big\}e^{j2\pi l'm/M}$$
$$= p_{i,k}[l]e^{j2\pi lm/M}\delta_{kk'} + \sigma_{\text{et}}^2 e^{j2\pi lm/M}\delta_{kk'}. \tag{47}$$

Substituting (47) in (46), leads to

$$\hat{h}_{k,k',m}^{(\text{eqvlt})}[l] \to h_{k,k',m}^{(\text{eqvlt})}[l] + \frac{N\sigma_{\text{et}}^2 \sqrt{\mu_k}\delta_{kk'}}{\sum_{i=0}^{N-1} \beta_{i,k} + N\sigma_{\text{ef}}^2}e^{j2\pi lm/M}. \tag{48}$$

Similar to the co-located setup in the previous subsection, here, subtracting the *correction factor* $\frac{N\sigma_{\text{et}}^2 \sqrt{\mu_k}\delta_{kk'}}{\sum_{i=0}^{N-1} \beta_{i,k} + N\sigma_{\text{ef}}^2}e^{j2\pi lm/M}$ from the equivalent channel estimate (45) and designing the equalizer based on the modified channel estimate, mitigates the channel estimation error effects. This statement is confirmed through computer simulations in the following section.

VI. Simulation Results

In this section, we evaluate our mathematical developments throughout the paper by computer simulations. We first present a set of results for a single cell scenario with co-located antennas at the BS. Then, simulation results that evaluate the performance of the proposed methods in a cell-free scenario are presented.

A. Single cell scenario

We consider QAM (quadrature amplitude modulation) symbols to be transmitted over $M = 64$ subcarriers of the SMT system with PHYDYAS prototype filter, [44], and overlapping factor $\kappa = 4$. In our simulations, we use tap delay line-C (TDL-C) 5G channel model, [45]. This model provides a PDP based on a normalized root mean square (RMS) delay spread. Following the instructions in [45], we randomly scale the normalized RMS delay spreads for different users in each simulation instance using a uniform distribution to achieve the RMS delay spreads within the range [90 ns, 110 ns], i.e., for channels with moderate lengths. The reason for this is that in realistic scenarios, PDPs between the users and the BS antennas are different. Perfect power control is assumed and, thus, the PDPs are normalized, i.e., we let $\sum_{l=0}^{L-1} p_k[l] = 1$ for $k = 0, \ldots, K - 1$. We consider the input signal-to-noise ratio (SNR) of 10 dB at the BS antennas unless otherwise is stated. We set the sampling frequency to 15.36 MHz. This

leads to the subcarrier spacing of 240 kHz, which is inline with 5G NR specifications, [45]. We have obtained our results for 1000 independent realizations of the channel with $K = 4$ users.

The URLLC applications require the minimum possible delay. Thus, finding a minimum acceptable equalizer length is of a great importance. Fig. 4 shows the SINR performance of the PDP-based FSE design as L_{FSE} and the number of base station antennas, N, vary. The result when the FSE is absent is also presented. Our results show the efficacy of the proposed FSE technique in removing the SINR saturation problem of the single stage equalization, i.e., the one with linear combining only. We also note that since in OFDM the channel is frequency flat over each subcarrier band, OFDM may be used as a benchmark for evaluating the efficacy of the proposed two-stage equalization. For the first stage, we consider ZF. For the channel scenario that is studied here, we find that an FSE length of $L_{\text{FSE}} = 3$ leads to a significant improvement over the case where there is no FSE. The improvement approaches the performance of OFDM for $L_{\text{FSE}} = 9$ and a minor deviation from this optimal performance is observed as L_{FSE} decreases to the values of 7 and 5. It appears that in the present channel scenario $L_{\text{FSE}} = 5$ strikes a good balance between the receiver complexity and latency, as well as its performance. Examining other channel models, we have found that this compromise choice remains the same over a wide range of channel conditions. Compared to the FSE design presented in [6], where $L_{\text{FSE}} = 345$, this FSE length is two orders of magnitude smaller. The need for a very long FSE in [6] was an outcome of using the brick-wall antialiasing filter that was mentioned in Section IV.

In Fig. 5, we compare the uncoded bit error rate (BER) performance of the FSE with different lengths in a scenario with $N = 100$ BS antennas and the constellation size of 64-QAM. From Fig. 5, one may realize that using the proposed FSE brings a significant BER performance improvement even when $L_{\text{FSE}} = 3$. It is worth noting that for SNRs up to 5 dB, the BER performance when $L_{\text{FSE}} = 3$ is very close to those with a longer L_{FSE}. At higher SNRs, this short equalizer leads to a loss of less than 1 dB at the BER of 10^{-6}. Based on these results, in the following experiments, we set $L_{\text{FSE}} = 5$.

In Fig. 6, we evaluate the performance of our proposed FSE with the length $L_{\text{FSE}} = 5$ for different designs. The designs that are presented are: (i) based on the equivalent channel (28); (ii) based on the exact PDP that has been used to generate the random channels; and (iii) based on the approximate/estimated PDP (40). It is also assumed that the channel estimates are perfect. These results show that the proposed FSE using the equivalent channel and the exact PDP lead to about the same performance. This is while the proposed FSE with the approximate/estimated PDP leads to a negligible performance loss. This loss is only observable for a large number of BS antennas where the output SINR approaches a large value and noise effects are no longer dominant. These results show that when the second order statistics of the channel is available at the BS, the computational burden for calculation of the exact equivalent channel that needs to be treated separately at different subcarriers can be avoided.
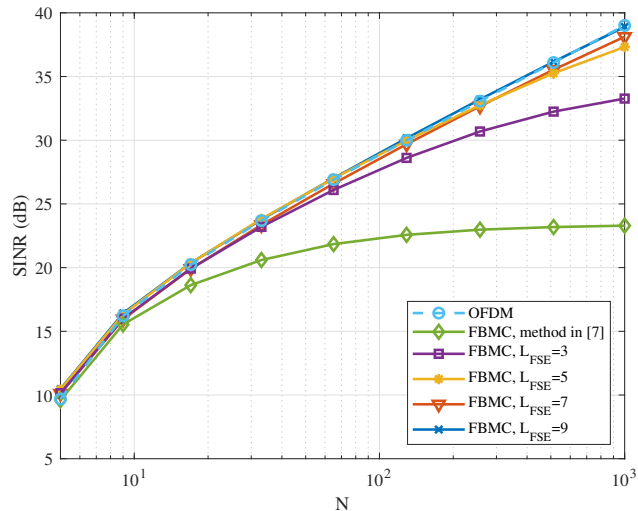
Fig. 4. SINR vs. the number of BS antennas, N. The BS antennas are co-located and FSE design is based on the PDP of the underlying channels. Different choices of L_{FSE} are examined. OFDM results are presented as a benchmark.
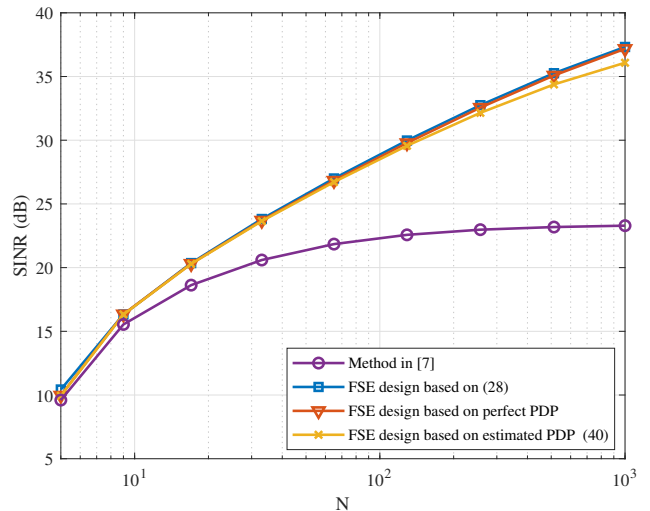

Fig. 6. Output SINR vs. the number of BS antennas, N, for different FSE designs. Perfect CSI is assumed and $L_{\mathrm{FSE}} = 5$.

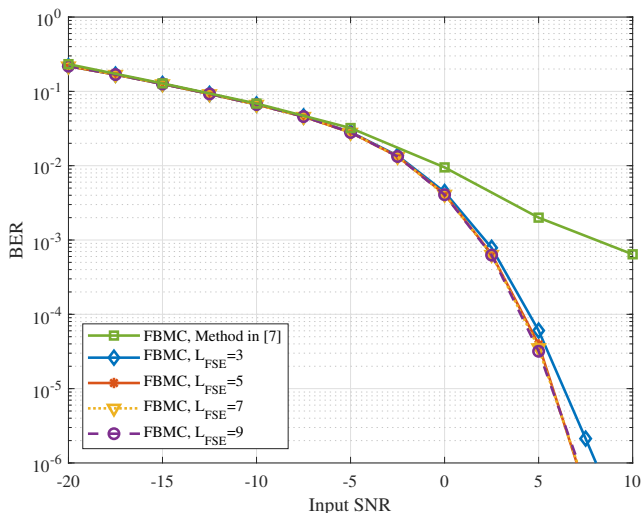Fig. 5. BER vs. input SNR, for $N = 100$. The BS antennas are co-located and FSE design is based on the PDP of the underlying channels. Different choices of L_{FSE} are examined.

Fig. 7. Output SINR vs. the number of BS antennas, N, for different FSE designs. $L_{\mathrm{FSE}} = 5$.

To study the imperfect CSI scenario, our proposed channel estimation method in Section III is deployed. We insert $\kappa-1 = 3$ guard symbols in time to isolate the preamble from the data symbols. Considering the imperfect CSI statistics, in Fig. 7, we study the efficacy of the proposed modified equalizers in Section V. These results show that the modified equalizers lead to an improved performance compared with the ones in Section IV that do not take into account the imperfect CSI effects. According to the results of Fig. 7, as the number of BS antennas increases, imperfect CSI effects become more problematic if not compensated.

Noting that channel estimation errors leading to imperfect CSI depend on the noise level at the input of BS antennas, in
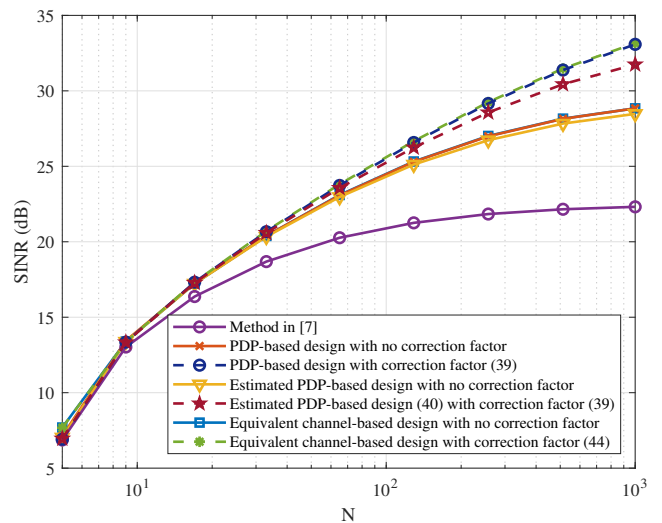
Fig. 8, we use estimated channels and study the output SINR as a function of the input SNR for $N = 200$. Our results in this figure show that as the input SNR increases, hence, noise level decreases, channel estimates become more accurate, and thus, the equalizers of Section IV achieve a similar performance to the modified ones in Section V. On the other hand, at lower values of SNR, the proposed modifications in Section V can lead up to 6 dB SINR improvement. Last but not least, while the single-stage equalization (i.e., linear combining only) leads to about the same performance as the two-stage equalization in the low SNR regime, the addition of the FSE (the second stage) can lead to a gain of 10 dB or more at higher values of SNR.
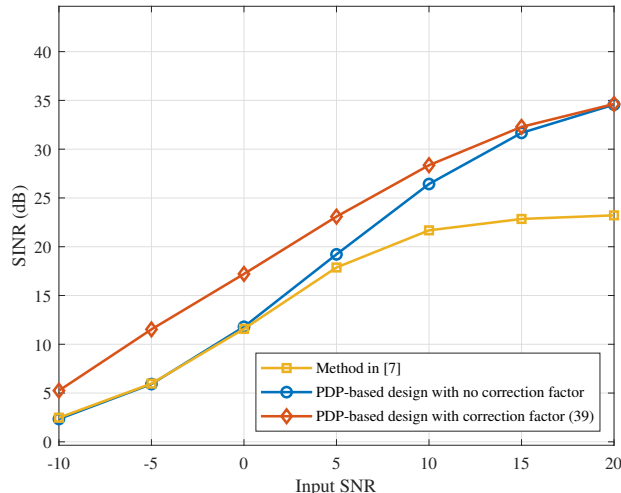
Fig. 8. Output SINR vs. input SNR.

Fig. 9. Comparison of the empirical CDF of OFDM and FBMC while using maximum power and power control.

B. Cell-free scenario

We perform simulations for a cell-free massive MIMO setup with APs that are located on a regular grid in a 2×2 square kilometers area. Each AP has 4 antennas. We deploy the wrap-around technique of [35] to imitate an infinite area and thus, avoid boundary effects. We consider $K = 4$ users that take random locations in each realization. We consider the same PDPs as the co-located setup. However, to take into account the distribution of antennas/APs, large-scale fading coefficients are added to different channels. The large-scale fading coefficients are modeled according to the COST Hata model as [46]

$$10\log_{10}(\beta_{i,k}) = -135 - 35\log_{10}(d_{i,k}) - \mathcal{X}_{i,k}, \qquad (49)$$

where $d_{i,k} > 10$ m is the distance between a given user k and antenna i in kilometers and $\mathcal{X}_{i,k} \sim \mathcal{CN}(0, \sigma_{\mathcal{X}}^2)$ represents shadowing effect with $\sigma_{\mathcal{X}}^2 = 8$ dB. Variance of noise is calculated using the noise figure as $\sigma_{\eta}^2 = \mathcal{K} \times \kappa_B \times B \times \text{NF}$, where $\mathcal{K}$, κ_B, B, and NF are temperature in kelvin, Boltzmann constant, bandwidth, and noise figure, respectively. Here, we let $\mathcal{K} = 290$ K, $\kappa_B = 1.3 \times 10^{-23}$ J/K, $B = 20$ MHz and NF $= 9$ dB. The maximum transmit power of each user is assumed to be 200 mW.

Fig. 9 illustrates the cumulative distribution function (CDF) of the signal-to-interference ratio (SIR) performance for FBMC- and OFDM-based cell-free MIMO setup having 9 APs in an area of 2×2 km and 4 users with and without power control, i.e., $\nu = 0$ and $\nu = 1$, respectively. The results show that power control leads to more stable values (i.e., less variation) in SIRs. This is inline with the previous results on OFDM in the literature [42]. Our results, here, confirm that the same is true for FBMC, and power control has almost the same impact on both OFDM and FBMC. Following the recommendations made in the literature, [41], [43] and [42], in the rest of this section, we consider the fractional power control with $\nu = 0.5$.
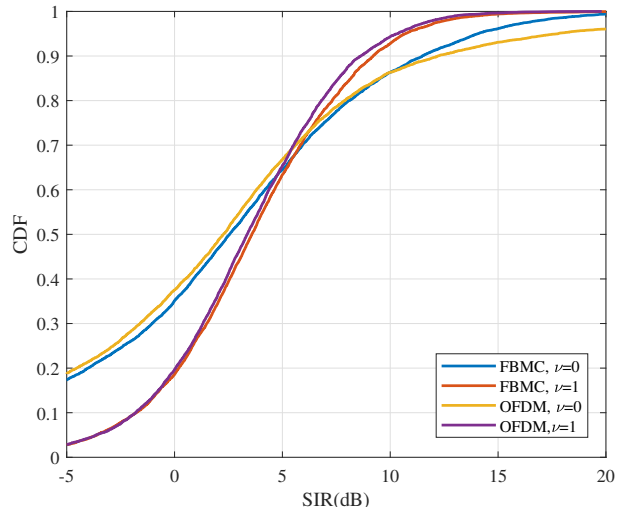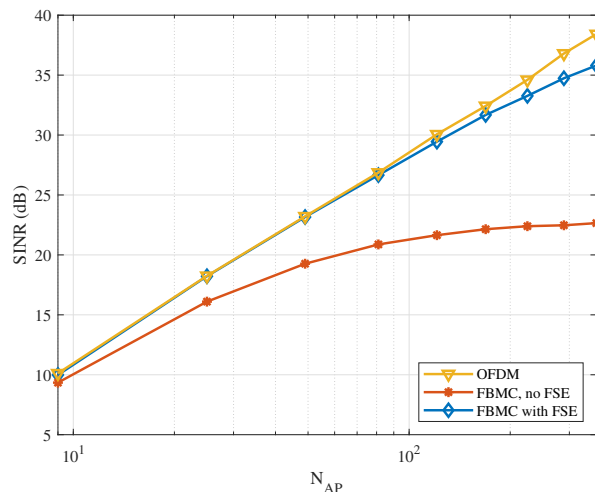

Fig. 10. Output SINR vs. number of APs, N_{AP}, for FSE design $L_{\text{FSE}} = 5$.

In Fig. 10, the SINR of our proposed two-stage FBMC receiver is compared with an OFDM system, as a benchmark. Here, the FSE has a length of $L_{\text{FSE}} = 5$. CSI is assumed to be known perfectly, and a ZF combiner is used as the first equalization stage at the FBMC receiver. The close performance of FBMC to OFDM confirms its efficacy. The small deviation of FBMC from OFDM, here, is attributed to the short length $L_{\text{FSE}} = 5$. It can be resolved by increasing L_{FSE} to 9, as in Fig. 4.

Fig. 11 presents simulation results for a case where CSI is estimated. The improvement that results from the correction term in (48) is also shown. Compared to the case of co-located antennas, the amount of improvement is relatively small. This difference may be attributed to the fact that in a distributed antenna/cell-free scenario, the number of effective antennas that serve each user remains small, no matter how large the total number of antennas or the number of APs will be. The
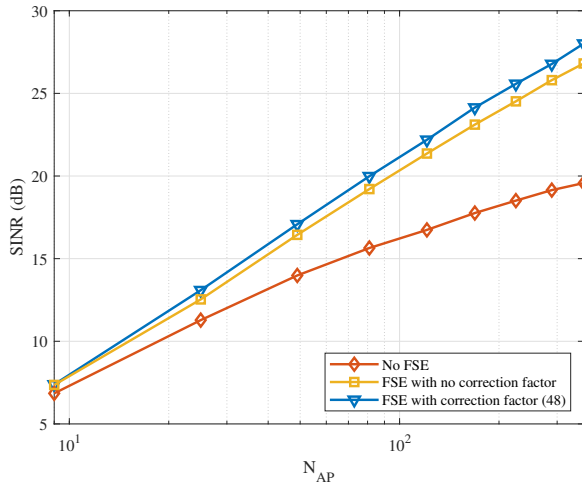
Fig. 11. Output SINR vs. number of APs, N_{AP}, for FSE design $L_{\text{FSE}} = 5$.

SINR improvement that is seen in Fig. 11 as N_{AP} increases is due to the fact that for large values of N_{AP}, there are always one or more APs near each user. Hence, the input SNR improves as the number of effective antennas increases.

VII. CONCLUSION

In this work, we designed practical receivers for FBMC-based massive MIMO in both co-located and distributed antenna setups with perfect/imperfect knowledge of CSI. We proposed a spectrally efficient channel estimation method that acquires the channel impulse responses of all the users jointly. Channel estimation error statistics were also calculated and utilized to improve the receiver designs. We proposed a two-stage equalization technique to improve on the performance of the FBMC-based massive MIMO systems. The proposed design consists of a linear combiner followed by a set of FSEs, i.e., one for each subcarrier of each user. We studied three different designs of the FSE. These designs may be thought of as modifications to a previously published work in our group, taking into account a number of needs in practical applications. The emphasis was to (i) reduce the FSE length, hence, save on the computational complexity and minimize the receiver processing latency; (ii) introduce new designs that are applicable to the more general applications, including distributed antenna systems and the recently proposed cell-free network architecture; (iii) take into account the channel estimation errors. Finally, we demonstrated the successful performance of the proposed designs through extensive numerical results.

APPENDIX A
FSE DERIVATION

In this appendix, we derive the FSE based on a MMSE-based technique that can achieve the optimal performance. In our derivations, we take a similar approach to [47] and [48], and the exact equivalent channel after single-tap combining, the PDP or its estimate is used as the input to the MMSE equalizer.

Here, we provide PDP-based FSE derivation. It is worth noting that PDP can be straightforwardly replaced with its estimate in (40) or the equivalent channel that was calculated in (28). From (20) and (21), we can obtain the time domain residual channel after combining as

$$g_{mm'}^{k,k}[n] = \sum_{i=0}^{N-1} W_m^{i,k}(f_{m'}[l] \star p_k[l]e^{j2\pi lm/M} \star f_m^*[-l])_{\downarrow \frac{M}{2}},$$
(50)

with the length of $L_g = (\lfloor \frac{2\kappa M+L-2}{M/2} \rfloor + 1)$, where κ is the overlapping factor of the prototype filter. Thus, the demodulated symbol of a given user k after combining, and before taking the real part and phase adjustment in the time-frequency bin (n, m) is obtained as

$$y_m^k[n] = \sum_{m'=m-1}^{m+1} \sum_{n'=-L_g/2}^{L_g/2-1} g_{mm'}^{k,k}[n']\gamma_m^k[n-n']$$
$$+ \sum_{i=0}^{N-1} W_m^{i,k}\Big(\sum_{n'=-\infty}^{+\infty} f_m^*[n-n']\eta_i[n']\Big)_{\downarrow \frac{M}{2}},$$
(51)

where $\gamma_m^k[n] = e^{j(m+n)\frac{\pi}{2}}s_{m,n}^k$. Let us consider a time domain per-subcarrier per-user equalizer $\phi_{m,k}$, with the length L_ϕ. Thus, the equalizer input for a given user, k, consists of L_ϕ demodulated samples that we stack in the vector $\mathbf{y}_m^k[n] = \big[y_m^k[n+\frac{L_\phi}{2}-1], \ldots, y_m^k[n-\frac{L_\phi}{2}]\big]^{\text{T}}$. Assuming $L_t = L_g + L_\phi$ and using (51), we can represent the vector $\mathbf{y}_m^k[n]$ as

$$\mathbf{y}_m^k[n] = \sum_{m'=m-1}^{m+1} \boldsymbol{\mathcal{G}}_{mm'}^{k,k}\boldsymbol{\gamma}_{m'}^k[n] + \sum_{i=0}^{N-1} W_m^{i,k}\boldsymbol{\Psi}_m\boldsymbol{\eta}_i[n\tfrac{M}{2}],$$
(52)

where $\boldsymbol{\mathcal{G}}_{m,m'}^{k,k} = \mathcal{T}_{L_\phi \times L_t}\big([g_{m,m'}^{k,k}[-\frac{L_g}{2}], \ldots, g_{m,m'}^{k,k}[\frac{L_g}{2}-1], \mathbf{0}_{1\times L_\phi}]\big)$, $\boldsymbol{\gamma}_m^k[n] = \big[\gamma_m^k[n+\frac{L_t}{2}-1], \ldots, \gamma_m^k[n-\frac{L_t}{2}]\big]^{\text{T}}$ is the vector of L_t transmitted symbols by user k at subcarrier m, and $\boldsymbol{\eta}_i[n\frac{M}{2}] = \big[\eta_i[n\frac{M}{2}], \eta_i[n\frac{M}{2}-1], \ldots, \eta_i[n\frac{M}{2}-(L_\phi' + \kappa M + 1)]\big]^{\text{T}}$, where $L_\phi' = (L_\phi - 1)\frac{M}{2}$. The matrix $\boldsymbol{\Psi}_m = \boldsymbol{\mathcal{D}}\mathcal{T}_{L_\phi' \times (L_\phi' + \kappa M)}\big([f_m^*[-\kappa\frac{M}{2}], \ldots, f_m^*[\kappa\frac{M}{2}-1], \mathbf{0}_{1\times L_\phi'}]\big)$ performs receiver filtering and decimation operations on noise vector, where decimation matrix $\boldsymbol{\mathcal{D}}$ is formed by the rows of identity matrix of size $\frac{M}{2}L_\phi$ with the indices that are integer multiples of $\frac{M}{2}$.

The equalizer output at time n can be obtained as $\tilde{\gamma}_m^k[n] = \phi_{m,k}^{\text{H}}\mathbf{y}_m^k[n]$. For the time-frequency symbol indices, m and n, where $(m+n)$ is even and odd, the real and imaginary parts of the equalizer output, respectively, provide the estimates of the transmit symbols. As it is shown in [47], the MMSE equalizers for pure imaginary and pure real symbols are identical. Here, we consider the pure real case in the following, leading to the equalizer output

$$\Re\{\tilde{\gamma}_m^k[n]\} = \Re\{\phi_{m,k}^{\text{H}}\mathbf{y}_m^k[n]\}$$
$$= \Re\{\phi_{m,k}^{\text{T}}\}\Re\{\mathbf{y}_m^k[n]\}$$
$$+ \Im\{\phi_{m,k}^{\text{T}}\}\Im\{\mathbf{y}_m^k[n]\}. \quad (53)$$

Due to the specific structure of SMT, the elements of $\boldsymbol{\gamma}_m^k[n]$ are pure real or imaginary. The real and imaginary parts of

the demodulated symbols, respectively, can be expanded as

$$\Re\{\mathbf{y}_m^k[n]\} = \sum_{m'=m-1}^{m+1} \Re\{\bar{\boldsymbol{\mathcal{G}}}_{mm'}^{k,k}\}\bar{\gamma}_{m'}^k[n]$$
$$+ \Re\{\boldsymbol{\Psi}_m \bar{\boldsymbol{\eta}}_{m,k}[n\tfrac{M}{2}]\} \qquad (54)$$

and

$$\Im\{\mathbf{y}_m^k[n]\} = \sum_{m'=m-1}^{m+1} \Im\{\bar{\boldsymbol{\mathcal{G}}}_{mm'}^{k,k}\}\bar{\gamma}_{m'}^k[n]$$
$$+ \Im\{\boldsymbol{\Psi}_m \bar{\boldsymbol{\eta}}_{m,k}[n\tfrac{M}{2}]\}, \qquad (55)$$

where $\bar{\boldsymbol{\mathcal{G}}}_{mm'}^{k,k}$ is formed by moving j from pure imaginary elements of $\gamma_m^k[n]$ to the corresponding columns of $\boldsymbol{\mathcal{G}}_{mm'}^{k,k}$, and note that $\bar{\gamma}_m^k[n] = \Re\{\gamma_m^k[n]\}$ and the elements of the noise vector $\bar{\eta}_{m,k}[n]$ have the variance of $\sigma_{\bar{\eta}_{m,k}}^2 = \sum_{i=0}^{N-1} |W_m^{i,k}|^2\sigma_\eta^2$. Using (53), the equalizer output can be rearranged as

$$\Re\{\tilde{\gamma}_m^k[n]\} = \tilde{\boldsymbol{\phi}}_{m,k}^{\mathrm{T}}\tilde{\mathbf{y}}_m^k[n]$$
$$= \tilde{\boldsymbol{\phi}}_{m,k}^{\mathrm{T}}\Bigg(\sum_{m'=m-1}^{m+1} \breve{\boldsymbol{\mathcal{G}}}_{m,m'}^{k,k}\bar{\gamma}_{m'}^k[n]$$
$$+ \breve{\boldsymbol{\Psi}}_m \breve{\boldsymbol{\eta}}_{m,k}[n\tfrac{M}{2}] \Bigg), \qquad (56)$$

where

$$\tilde{\boldsymbol{\phi}}_{m,k} = \begin{bmatrix} \Re\{\boldsymbol{\phi}_{m,k}\} \\ \Im\{\boldsymbol{\phi}_{m,k}\} \end{bmatrix}, \qquad \tilde{\mathbf{y}}_m^k[n] \begin{bmatrix} \Re\{\mathbf{y}_m^k[n]\} \\ \Im\{\mathbf{y}_m^k[n]\} \end{bmatrix},$$

$$\breve{\boldsymbol{\mathcal{G}}}_{mm'}^{k,k} = \begin{bmatrix} \Re\{\bar{\boldsymbol{\mathcal{G}}}_{mm'}^{k,k}\} \\ \Im\{\bar{\boldsymbol{\mathcal{G}}}_{mm'}^{k,k}\} \end{bmatrix}, \qquad \breve{\boldsymbol{\eta}}_{m,k}[n\tfrac{M}{2}] = \begin{bmatrix} \Re\{\bar{\boldsymbol{\eta}}_{m,k}[n\tfrac{M}{2}]\} \\ \Im\{\bar{\boldsymbol{\eta}}_{m,k}[n\tfrac{M}{2}]\} \end{bmatrix},$$

and

$$\breve{\boldsymbol{\Psi}}_m = \begin{bmatrix} \Re\{\boldsymbol{\Psi}_m\} & -\Im\{\boldsymbol{\Psi}_m\} \\ \Im\{\boldsymbol{\Psi}_m\} & \Re\{\boldsymbol{\Psi}_m\} \end{bmatrix}.$$

Thus, the MMSE equalizer $\tilde{\boldsymbol{\phi}}_{m,k}$ can be found by minimizing

$$\mathbb{E}[|\tilde{\boldsymbol{\phi}}_{m,k}^{\mathrm{T}}\tilde{\mathbf{y}}_m^k[n] - \gamma_m^k[n - \Delta_{m,k}]|^2], \qquad (57)$$

where $\Delta_{m,k}$ is the equalizer delay, [47]. By setting derivatives of (57) with respect to $\tilde{\boldsymbol{\phi}}_{m,k}$ equal to zero, the optimum equalizer tap-weight vector is obtained as

$$\tilde{\boldsymbol{\phi}}_{m,k} = \Bigg(\sum_{m'=m-1}^{m+1} \breve{\boldsymbol{\mathcal{G}}}_{mm'}^{k,k}(\breve{\boldsymbol{\mathcal{G}}}_{mm'}^{k,k})^{\mathrm{T}} + \sigma_{\bar{\eta}_{m,k}}^2 \breve{\boldsymbol{\Psi}}_m \breve{\boldsymbol{\Psi}}_m^{\mathrm{T}} \Bigg)^{-1}$$
$$\times \breve{\boldsymbol{\mathcal{G}}}_{mm}^{k,k}\boldsymbol{\delta}_{m,k}, \qquad (58)$$

where $\boldsymbol{\delta}_{m,k}$ is the vector of all zeros except at the element $\Delta_{m,k}$ which is 1.

REFERENCES

[1] H. Tataria, M. Shafi, A. F. Molisch, M. Dohler, H. Sjöland, and F. Tufvesson, "6G wireless systems: Vision, requirements, challenges, insights, and opportunities," *arXiv preprint arXiv:2008.03213*, 2020.

[2] B. Farhang-Boroujeny, "OFDM versus filter bank multicarrier," *IEEE signal processing magazine*, vol. 28, no. 3, pp. 92–112, 2011.

[3] R. Nissel, S. Schwarz, and M. Rupp, "Filter bank multicarrier modulation schemes for future mobile communications," *IEEE Journal on Selected Areas in Communications*, vol. 35, no. 8, pp. 1768–1782, 2017.

[4] B. Farhang-Boroujeny, "Filter bank multicarrier modulation: A waveform candidate for 5G and beyond," *Advances in Electrical Engineering*, 2014.

[5] A. Aminjavaheri, A. Farhang, N. Marchetti, L. E. Doyle, and B. Farhang-Boroujeny, "Frequency spreading equalization in multicarrier massive MIMO," in *2015 IEEE International Conference on Communication Workshop (ICCW)*. IEEE, 2015, pp. 1292–1297.

[6] A. Aminjavaheri, A. Farhang, and B. Farhang-Boroujeny, "Filter bank multicarrier in massive MIMO: Analysis and channel equalization," *IEEE Transactions on Signal Processing*, vol. 66, no. 15, pp. 3987–4000, 2018.

[7] A. Farhang, N. Marchetti, L. E. Doyle, and B. Farhang-Boroujeny, "Filter bank multicarrier for massive MIMO," in *2014 IEEE 80th vehicular technology conference (VTC2014-Fall)*. IEEE, 2014, pp. 1–7.

[8] F. Rottenberg, X. Mestre, F. Horlin, and J. Louveaux, "Performance analysis of linear receivers for uplink massive MIMO FBMC-OQAM systems," *IEEE Transactions on Signal Processing*, vol. 66, no. 3, pp. 830–842, 2018.

[9] P. Singh, H. B. Mishra, A. K. Jagannatham, K. Vasudevan, and L. Hanzo, "Uplink sum-rate and power scaling laws for multi-user massive MIMO-FBMC systems," *IEEE Transactions on Communications*, vol. 68, no. 1, pp. 161–176, 2019.

[10] P. Schulz, M. Matthe, H. Klessig, M. Simsek, G. Fettweis, J. Ansari, S. A. Ashraf, B. Almeroth, J. Voigt, I. Riedel *et al.*, "Latency critical IoT applications in 5G: Perspective on the design of radio interface and network architecture," *IEEE Communications Magazine*, vol. 55, no. 2, pp. 70–78, 2017.

[11] C. Lélé, J.-P. Javaudin, R. Legouable, A. Skrzypczak, and P. Siohan, "Channel estimation methods for preamble-based OFDM/OQAM modulations," *European Transactions on Telecommunications*, vol. 19, no. 7, pp. 741–750, 2008.

[12] E. Kofidis, D. Katselis, A. Rontogiannis, and S. Theodoridis, "Preamble-based channel estimation in OFDM/OQAM systems: A review," *Signal processing*, vol. 93, no. 7, pp. 2038–2054, 2013.

[13] M. Caus and A. I. Pérez-Neira, "Transmitter-receiver designs for highly frequency selective channels in MIMO FBMC systems," *IEEE Transactions on Signal Processing*, vol. 60, no. 12, pp. 6519–6532, 2012.

[14] E. Kofidis, "Preamble-based channel estimation in FBMC/OQAM systems: A time-domain approach," *arXiv preprint arXiv:1306.2581*, 2013.

[15] ——, "Short preamble-based estimation of highly frequency selective channels in FBMC/OQAM," in *2014 IEEE International Conference on Acoustics, Speech and Signal Processing (ICASSP)*. IEEE, 2014, pp. 8058–8062.

[16] D. Kong, D. Qu, and T. Jiang, "Time domain channel estimation for OQAM-OFDM systems: Algorithms and performance bounds," *IEEE Transactions on Signal Processing*, vol. 62, no. 2, pp. 322–330, 2014.

[17] E. Kofidis, "Preamble-based estimation of highly frequency selective channels in FBMC/OQAM systems," *IEEE Transactions on Signal Processing*, vol. 65, no. 7, pp. 1855–1868, 2017.

[18] K. Zhang and L. Xue, "Iterative weight LS channel estimation in time domian for OQAM/OFDM systems," in *2017 3rd IEEE International Conference on Computer and Communications (ICCC)*. IEEE, 2017, pp. 158–161.

[19] E. Kofidis, "Preamble-based estimation of highly frequency selective channels in MIMO-FBMC/OQAM systems," in *Proceedings of European wireless 2015; 21th European wireless conference*. VDE, 2015, pp. 1–6.

[20] P. Singh and K. Vasudevan, "Time domain channel estimation for MIMO-FBMC/OQAM systems," *Wireless Personal Communications*, pp. 1–20, 2019.

[21] E. Kofidis, "Preamble-based FBMC/OQAM channel estimation without guard symbols," Jul. 2020, working paper or preprint. [Online]. Available: https://hal.archives-ouvertes.fr/hal-02889973

[22] K. Chen-Hu, J. C. Estrada-Jimenez, M. J. Fernandez-Getino Garcia, and A. G. Armada, "Superimposed training for channel estimation in FBMC-OQAM," in *2017 IEEE 86th Vehicular Technology Conference (VTC-Fall)*, 2017, pp. 1–5.

[23] F. Rottenberg, Y. Medjahdi, E. Kofidis, and J. Louveaux, "Preamble-based channel estimation in asynchronous FBMC-OQAM distributed MIMO systems," in *2015 International Symposium on Wireless Communication Systems (ISWCS)*. IEEE, 2015, pp. 566–570.

[24] M. Morelli and U. Mengali, "A comparison of pilot-aided channel estimation methods for OFDM systems," *IEEE Transactions on signal processing*, vol. 49, no. 12, pp. 3065–3073, 2001.

[25] F. Rusek, D. Persson, B. K. Lau, E. G. Larsson, T. L. Marzetta, O. Edfors, and F. Tufvesson, "Scaling up MIMO: Opportunities and challenges with very large arrays," *IEEE signal processing magazine*, vol. 30, no. 1, pp. 40–60, 2012.

[26] T. Ihalainen, A. Ikhlef, J. Louveaux, and M. Renfors, "Channel equalization for multi-antenna FBMC/OQAM receivers," *IEEE transactions on vehicular technology*, vol. 60, no. 5, pp. 2070–2085, 2011.

[27] F. Rottenberg, X. Mestre, F. Horlin, and J. Louveaux, "Single-tap equalizer for MIMO FBMC systems under doubly selective channels," in *2017 IEEE International Conference on Acoustics, Speech and Signal Processing (ICASSP)*. IEEE, 2017, pp. 3784–3788.

[28] E. Kofidis, C. Chatzichristos, and A. L. de Almeida, "Joint channel estimation/data detection in MIMO-FBMC/OQAM systems—A tensor-based approach," in *2017 25th European Signal Processing Conference (EUSIPCO)*. IEEE, 2017, pp. 420–424.

[29] M. Renfors, X. Mestre, E. Kofidis, and F. Bader, *Orthogonal waveforms and filter banks for future communication systems*. Academic Press, 2017.

[30] H. Q. Ngo, A. Ashikhmin, H. Yang, E. G. Larsson, and T. L. Marzetta, "Cell-free massive MIMO versus small cells," *IEEE Transactions on Wireless Communications*, vol. 16, no. 3, pp. 1834–1850, 2017.

[31] B. Hirosaki, "An analysis of automatic equalizers for orthogonally multiplexed QAM systems," *IEEE Transactions on Communications*, vol. 28, no. 1, pp. 73–83, 1980.

[32] H. Hosseiny, A. Farhang, and B. Farhang-Boroujeny, "Spectrally efficient pilot structure and channel estimation for multiuser FBMC systems," in *2020 IEEE International Conference on Communications (ICC): Wireless Communications Symposium (IEEE ICC'20 - WC Symposium)*, Dublin, Ireland, Jun. 2020.

[33] S. M. Kay, *Fundamentals of statistical signal processing*. Prentice Hall PTR, 1993.

[34] H. Q. Ngo, E. G. Larsson, and T. L. Marzetta, "Energy and spectral efficiency of very large multiuser MIMO systems," *IEEE Transactions on Communications*, vol. 61, no. 4, pp. 1436–1449, 2013.

[35] E. Björnson and L. Sanguinetti, "Making cell-free massive MIMO competitive with MMSE processing and centralized implementation," *IEEE Transactions on Wireless Communications*, 2019.

[36] S. U. H. Qureshi, "Adaptive equalization," *Proceedings of the IEEE*, vol. 73, no. 9, pp. 1349–1387, 1985.

[37] B. Farhang-Boroujeny, *Signal processing techniques for software radios*. Lulu publishing house, 2008, vol. 2.

[38] P. P. Vaidyanathan, *Multirate systems and filter banks*. Pearson Education India, 2006.

[39] B. Farhang-Boroujeny, *Adaptive filters: theory and applications*. John Wiley & Sons, 2013.

[40] E. Nayebi, A. Ashikhmin, T. L. Marzetta, and H. Yang, "Cell-free massive MIMO systems," in *2015 49th Asilomar Conference on Signals, Systems and Computers*. IEEE, 2015, pp. 695–699.

[41] A. Simonsson and A. Furuskar, "Uplink power control in LTE-overview and performance, subtitle: principles and benefits of utilizing rather than compensating for SINR variations," in *2008 IEEE 68th Vehicular Technology Conference*. IEEE, 2008, pp. 1–5.

[42] R. Nikbakht, R. Mosayebi, and A. Lozano, "Uplink fractional power control and downlink power allocation for cell-free networks," *IEEE Wireless Communications Letters*, vol. 9, no. 6, pp. 774–777, 2020.

[43] R. D. Yates, "A framework for uplink power control in cellular radio systems," *IEEE Journal on selected areas in communications*, vol. 13, no. 7, pp. 1341–1347, 1995.

[44] M. Bellanger, D. Le Ruyet, D. Roviras, M. Terré, J. Nossek, L. Baltar, Q. Bai, D. Waldhauser, M. Renfors, T. Ihalainen *et al.*, "FBMC physical layer: a primer," *Phydyas*, vol. 25, no. 4, pp. 7–10, 2010.

[45] T. ETSI, "138 901 v14. 0.0,"5G; study on channel model for frequencies from 0.5 to 100GHz," 3GPP TR 38.901 version 14.0. 0 Release 14)," ETSI, Tech. Rep., 2017.

[46] E. Damosso, L. M. Correia *et al.*, "COST action 231: Digital mobile radio towards future generation systems: Final report," *European commission*, 1999.

[47] A. Ikhlef and J. Louveaux, "An enhanced MMSE per subchannel equalizer for highly frequency selective channels for FBMC/OQAM systems," in *2009 IEEE 10th Workshop on Signal Processing Advances in Wireless Communications*. IEEE, 2009, pp. 186–190.

[48] D. W. M. Guerra and T. Abrão, "Efficient multitap equalization for FBMC-OQAM systems," *Transactions on Emerging Telecommunications Technologies*, vol. 30, no. 12, p. e3775, 2019.

Hamed Hosseiny (M' 19) received the B.S. in electrical engineering from Ferdowsi University of Mashhad, Iran, in 2013 and the M.S. in Electrical Engineering-Communication System-Network from the University of Tehran, Iran, in 2016. Since 2018, he has been working as a research assistant in the Wireless Communications Lab, pursuing a Ph.D. degree in electrical engineering at the University of Utah, USA. His research interests include Wireless Communications, Multicarrier Communications, Digital Signal Processing, and Cellular Networks.

Arman Farhang (SM' 2021) received the Ph.D. degree from Trinity College Dublin, Ireland, in 2016. He was a Research Fellow with CONNECT, Trinity College Dublin, Ireland, from 2016 to 2018 and an Assistant Professor at Maynooth University and University College Dublin in Ireland from 2018 to 2021. He is currently with the Electronic and Electrical Engineering Department at Trinity College Dublin as an Assistant Professor. He has published over 60 peer-reviewed international journal and conference papers, 4 book chapters, 1 edited book, and he holds 2 patents. His research interests include wireless communications, digital signal processing for communications, waveform design, multiuser communications, multiantenna and multicarrier systems. He serves as an Associate Editor of EURASIP Journal on Wireless Communications and Networking. He served as a member of the Organization Committee of the IEEE ICC 2020. He regularly serves as a TPC in top-tier IEEE conferences and workshops in addition to being an active reviewer of several major IEEE journals.

Behrouz Farhang-Boroujeny (M'84, SM'90, Life SM, 2017) received the B.Sc. degree in electrical engineering from Teheran University, Iran, in 1976, the M.Eng. degree from University of Wales Institute of Science and Technology, UK, in 1977, and the Ph.D. degree from Imperial College, University of London, UK, in 1981. From 1981 to 1989 he was with the Isfahan University of Technology, Isfahan, Iran. From 1989 to 2000 he was with the National University of Singapore. Since August 2000, he has been with the University of Utah.
He is an expert in the general area of signal processing. His current scientific interests are adaptive filters, multicarrier communications, detection techniques for space-time coded systems, and cognitive radio. In the past, he has worked and has made significant contribution to areas of adaptive filters theory, acoustic echo cancellation, magnetic/optical recoding, and digital subscriber line technologies. He is the author of the books "Adaptive Filters: theory and applications", John Wiley & Sons, 1998, and "Signal Processing Techniques for Software Radios", self published at Lulu publishing house, 2009 and 2010 (second edition). Dr. Farhang-Boroujeny received the UNESCO Regional Office of Science and Technology for South and Central Asia Young Scientists Award in 1987. He served as an associate editor of IEEE Trans. on Signal Processing from July 2002 to July 2005, and as an associate editor of IEEE Signal Processing Letters from April 2008 to March 2010. He has also been involved in various IEEE activities, including the chairmanship of the Signal Processing/Communications chapter of IEEE of Utah in 2004 and 2005.